Miniaturized non-back-drivable mechanism for robotic applications

Marco Controzzi, Christian Cipriani, and Maria Chiara Carrozza

The DOI of the final edited version of this paper is: 10.1016/j.mechmachtheory.2010.05.008

Miniaturized non-back-drivable mechanism for robotic applications

Marco Controzzi[†], Christian Cipriani and Maria Chiara Carrozza

ARTS-Lab (Advanced Robotics Technologies and Systems Laboratory), Scuola Superiore Sant'Anna, Polo Sant'Anna Valdera, Viale Rinaldo Piaggio, 34 - 56025 - Pontedera (PI), Italy,

{marco.controzzi,christian.cipriani,carrozza}@sssup.it

Abstract

Small actuators and high efficiency transmissions are essential components in mechatronic and robotic systems, since their performances affect overall volume, weight and power consumption. An innovative miniaturized, low cost, clutching mechanism for robot applications, based on wedge phenomenon in eccentric non-eccentric cam coupling has been designed, developed and evaluated. It is embedded into a human-size, robot hand prosthesis, allowing it to efficiently produce powerful grasps, but it could be employed in all those applications where strict power and weight-size constraints exist and a self-braking mechanism is required. High efficiency, compared to conventional non-back-drivable mechanisms based on screw lead-screw coupling, is achieved by means of roll cylinders inside the clutch. The system has been integrated with a DC motor and a capstan on which a tendon is wound, and then finally connected to the hand fingers. Detailed kinematics, static and dynamic analysis are presented as well as finite-element-method simulations and experimental measurements showing successful fulfilment of requirements. Maximum efficiency is about 0.95 in a large load range, the critical torque at which the mechanism unlocks is about 1 Nm.

Keyword: *Micro-Mechanisms, Clutch, Non-Back-Drivability, Robotics*

1. INTRODUCTION

The development of high energy storage capacity actuators and efficient transmission architectures is one of the key issues for the successful achievement of lightweight, efficient, and therefore functional robots. These features become more important in battery-powered systems, where energy-saving and harvesting convert into a longer working autonomy.

[†] Corresponding author. Phone: +39 050 883 460 - Fax: +39 050 883 497.E-mail: marco.controzzi@sssup.it

Within this framework, one of the most representative and challenging unresolved scientific problems is grasping and manipulation with robotic dexterous hands, prostheses and grippers, for which the actuator has been identified as the most serious long term impediment [1]. The idea of having dexterous manipulative, non task-specific robotic tools has been behind the interest shown by a number of research groups worldwide. The covered areas range from kinematics to actuation, to dynamic control of grasping and manipulation including design considerations [1]. When considering prosthetic applications, the multi-functionality of the prosthesis strongly depends on the performance of the actuator unit, since it will determine to a large extent the *autonomy* of the entire system, the available *grasping force*, the *weight* and *size*, and *aesthetic* issues like *noise* [1]. One of these properties is non-back-drivability: a transmission mechanism is defined as *non-back-drivable* when motion can be transmitted only from the input to the output axis and not vice-versa. Such property enables the actuator to deliver a stall torque without energy consumption, therefore the possibility to switch off the power, once a desired position of the hand or grasp stability has been achieved. Generally, in grippers and artificial hands, e.g. employed as end effectors for humanoid robots [2], [3], non-back-drivability is important for safety reasons; electrical supply or battery failures should not cause the (potentially dangerous) release of grasped objects or tools due to back-drivable transmissions. Moreover in grippers with high level of underactuation, the presence of a minimum number of non-back-drivable mechanisms is mandatory in order to produce first order form closure grasps [4].

Many non-back-drivable mechanisms and mechanical clutches have been developed in the past, and some have been miniaturized for robotic applications where constraints of weight and dimension do exist. In particular *lead-screw* (cf. Fig. 1a), and *worm gear* pairs (cf. Fig. 1b) have been employed. In these non-back-drivability is obtained due to shear friction involved during operation, and therefore their efficiency is very low. The mechanical efficiency of the backward motion ξ, in a common screw/lead screw or worm gear pair is defined as:

$$\xi \approx \frac{2\eta - 1}{\eta} \tag{1}$$

With η the mechanical efficiency of the direct motion. The non-back-drivable condition of $\xi < 0$ is assured with low direct efficiency $\eta \leq 0.5$ [5]. Even though, these mechanisms are easy to build and assemble, and have been successfully employed in several advanced prototypes like the Southampton hand [6], CyberHand [7], RTR II [8], TBM [9] and the recently (since 2007) commercially available i-Limb [10].

Figure 1

Non-back-drivability may also be achieved by means of *high reduction ratio* transmissions, where a large rotation of the motor is transformed into a small displacement of the end-effector. This in turn means that when a large force is applied to the end-effector it corresponds to a small torque on the motor, due to the principle of virtual work. Such a concept has been employed in prosthetic hand prototypes, e.g. in the Oxford [11] , the MARCUS [12] and the MANUS [1] hands. The main drawbacks are the high backlash, and consequent controllability problems, resulting from the number of gears and components involved in the transmission chain, and the necessity of finding a trade-off for obtaining suitable speed-torque performances. In order to obtain good performances, bulky motors could be required, resulting in a less dexterous hand, because of the unavailability of high power density commercial actuators.

Besides previous concepts, other kinds of non-back-drivable mechanisms not governed by Eq. (1) are present in literature [13]: these include *brakes* and mechanisms based on *wedge phenomena*.

Brakes, commonly employed in automotive, vehicular, and mobile robotic applications, are based on slip friction maximization between mobile surfaces connected to the transmission and finally to the load, and fixed surfaces rigidly fixed to the frame. The main drawback for their employment in robotic hands, grippers, or prostheses, is the requirement of extra energy for connecting (or disconnecting) the braking system.

The *free wheel* shown in Fig. 1c (employed for example in bicycle transmission or fishing reels) is a basic mechanism based on the coupling between a cam and rolling elements (spheres, cylinders, etc.), in which wedge phenomena are involved during the operation in one direction, stopping the torque transmission from the output to the input shaft. A conventional cam-ball clutch consists of an inner member, outer member, and rolling elements. The inner driving member has cam surfaces on opposite sides and carries spheres to either wedge or unwedge them. During the counter-clockwise rotation of the inner member, self-energizing friction forces the balls to tightly wedge between the inner and outer members. As a result, the outer and inner members are driven in the same direction. Conversely, if the inner member rotates clockwise or the outer member attempts to run ahead of the inner member, the balls move out of the tightly wedged position. Consequently the connection between the inner and outer members is broken. A system based on this mechanism has been recently employed in the KNU hand [14]. More complex systems based on wedge phenomena may be found in prosthetics: Ottobock Sensor-Hand (the market leader myoelectric prosthesis) [15] embeds a patented system integrated with the motor axis [16] combining a clutch with a two speed automatic transmission. The system automatically increases the pinch force (by increasing the transmission ratio) when high torque is required while grasping, and locks the fingers (thus maintaining the grasp) when the power is switched-off. Such a smart device represents a benchmark for engineers working in the field. Nevertheless, being so sophisticated, and integrated on its motor axis, as well as patented, preclude researchers for exploiting it in other designs or even to replicate it. Moreover,

it must be noted that it is composed of approximately 100 sub-parts, including elastic and rolling elements, therefore it cannot be defined as a simple, cheap device.

The objective of this work is the development of an innovative, (i) miniaturized, (ii) low-cost, (iii) high efficiency, (iv) easy to manufacture and assemble, non-back-drivable mechanism with (v) high efficiency. Such a system is currently embedded into a human-size, robot hand prosthesis, named SmartHand [17], allowing it to efficiently produce powerful grasps, but it could be employed in all those robotic applications where strict power and weight-size constraints exist and a self-braking mechanism is required.

In this paper the non-back-drivable mechanism (NBDM) developed, based on wedge phenomenon is presented. Detailed kinematics, static and dynamic analysis are presented and finite element method (FEM) simulation and experimental measurements in order to evaluate efficiency and performance of the system are reported and discussed.

2. MATERIALS AND METHODS

The NBDM described in this paper is based on the known mechanical concept presented in Fig. 2b. It is usually employed in dual motor/engine drivers, conveyor belts and pumps, and its volume can range between 200 to 500 cm^3 and above [18].

Figure 2

The system is composed of a fixed ring secured on the ground (1 in Fig. 2), an input shaft with two teeth (2), an eccentric cam (6) coaxial with the input shaft and fixed to the output shaft, and four brass cylinders (3, 4) that under the action of two compression springs, tend to wedge between the fixed ring and the cam. Both shafts are supported by two ball bearings. Referring to the picture, when the input shaft (i.e. the motor shaft) is rotated clockwise, the teeth (2) unblock the cylinders (4), if rotated anticlockwise, teeth (2) unblock the cylinders (3). In both cases an appendix of the two teeth drag the cam, and therefore the output shaft. The transmission from the output shaft (connected to the load) to the motor shaft is not allowed, since the cylinders (3) or (4) block the cam movement before teeth are contacted (and so dragged). A small gap between the cam and the motor shaft teeth is necessary for a correct operation; in order to prevent sliding friction, isolation between elastic elements and the fixed ring is also present. In order to choose the correct parameters of the design, a systematic method considering *kinematics*, *static* and *dynamic* analysis has been pursued.

2.1 Kinematics Analysis

In robotics and mechatronics the minimization of backlash motion within actuators or transmission systems is a very important issue to be carefully addressed in order to avoid/reduce control and stability problems. In underactuated robotic grippers zero backlash in the backward motion ensures the non-back-drivability condition and therefore form closure stability and high forces in power grasps [4]. In dexterous robotic hands or artificial prostheses this issue is even more important with regard to manipulating objects [19]. In order to minimize the backlash of the system under investigation a kinematics analysis has been performed. This implies a critical analysis of the inner clearances, micro-mechanics manufacturing processes and working principles of the mechanism.

Figure 3

The action of the compression springs that wedge the cylinders between the fixed ring and the cam, ensure (within certain deformation values) a zero backlash in the output shaft. This feature is very important with regards to the application of the mechanism in dexterous robotic hands and grippers [4], [19]. Backlash is present and unavoidable in the input shaft, since for a proper operation of the mechanism some inner clearances are required. Torque is transmitted from the motor to the output shaft in two steps: firstly the input shaft must rotate sufficiently to put the teeth in contact with the cylinders (cover the angular gap g_1 in Fig. 3b); secondly cylinders must be unlocked and the input shaft must additionally rotate until the appendix gets in contact with the output shaft, i.e. cover gap g_2 (that includes gap g_1, Fig. 3c). This is the backlash of the system. In the first step, theoretically, teeth and cylinders can be in contact or almost in contact; in other words gap g_1 can be reduced to a theoretical limit of zero, if we suppose that the mechanism is locked under the action of the compression springs. In practice, a minimum angular gap g_1 (or, linear gap h_1) is necessary because of (i) the uncertain location of the cylinders in the lock configuration, which is determined by the drilling machine tolerance (i.e. accuracy of the manufacturing process) and (ii) the strain of the components due to applied loads.

In the second step (Fig. 3c), cylinders are unlocked and the cam shaft and the appendix of the motor shaft get in contact therefore transmitting the torque to the output. This gap g_2, is both theoretically and practically needed, and since it is strictly connected to the interference between cylinders and the fixed ring, it is influenced by the previous g_1.

Considering Fig. 2b the distance between the fixed ring and cam surfaces is defined as δ :

$$\delta = -r_c + \sqrt{e^2 + r_f^2 - 2er_f \cos(\phi - \vartheta)} \tag{2}$$

Where e is the eccentricity of the cam, r_c is the radius of the cam, r_f is the radius of the fixed ring and θ is the angle between the vertical axis and the axis through the middle axis of the mechanism and the external surface of the cylinder

(cf. Fig. 2b). Such δ decreases with θ as shown in the left graph of Fig. 4. If the radius of the cylinders r_s is known, by imposing δ equal to 2 r_s (cylinders diameter) in Eq. 2a relation between r_s and θ is found.

Figure 4

Gap h_1 and g_1 are functions of θ as shown in the right graph of Fig. 4 and are calculated as follows:

$$g_1 = \beta - \vartheta \tag{3}$$

$$g_1 = (r_f - r_s) \approx h_1 \approx \beta(r_f - r_s) - [\vartheta(r_f - r_s)] \tag{4}$$

$$g_1 \approx \frac{h_1}{r_f - r_s} \tag{5}$$

If we define r_a as the distance between the middle axis of the mechanism and the contact point between the cam and the teeth, the total backlash g_2 is simply:

$$g_2 \approx \frac{h_2}{r_a} \tag{6}$$

In order to have a correct operation it is necessary that $h_2 > h_1$; a safety factor taking into account the accuracy of manufacturing process and alignment errors due to ball bearing tolerances must therefore be considered in combination with the results obtained from the following static and dynamic analyses.

2.2 Static Analysis

A static analysis has been conducted in order to investigate contact pressures on the involved surface pairs with the aim of reducing the size and weight of the components. In this analysis the presence of compression springs has been neglected, according to the real situation where the force they apply on the cylinders (several Newtons) is one order lower than the static reaction applied by the external load (tens of Newtons while grasping, hundreds of Newtons in overload condition) [5], [20].

H. Hertz developed the mathematical theory for investigating surfaces stress and deformation produced by the pressure generated between two curved bodies [21]. Using equations based on Hertz theory the theoretical contact pressures on the cam-cylinder $P_{s\text{-}c}$ and the cylinder-fixed ring interfaces $P_{s\text{-}f}$ have been calculated, as well as the maximum shear stress beneath the surfaces of the fixed ring and the cylinders [20], [21], as shown by Eq. 7:

$$P_{s-i} = 0{,}564\sqrt{\frac{P_0(1/r_s + 1/r_i)}{l\Delta}} \quad \text{with} \quad i = c, f \tag{7}$$

where P_0 is the load on the cylinder, Δ is defined as:

$$\Delta = \frac{1-\nu_1^2}{E_1} + \frac{1-\nu_2^2}{E_2} \tag{8}$$

and $\nu_{1,2}$, $E_{1,2}$ are respectively the Poisson's ratio and the Young's modulus for the two pairs of materials chosen.

Figure 5

Under static load condition, rolling elements such as spheres increase contact pressures due to limited contact areas; cylinders represent a better choice (also considering the miniaturized dimensions). In Fig. 5a the theoretical contact pressures, for different materials, as a function of the radius of the cylinder is presented. According to Hertz theory then, an optimal radius for which contact pressures in ring-cylinder and cam-cylinder interfaces are equal and properly scaled, is found (r_s = 1.5 mm). This result is true only using brass cylinders and stainless steel ring and cam. Such a choice is consistent with wear issues (related to the hardness of materials): since steel is harder [5], [20], once ruined, brass cylinders may be easily replaced at low cost.

A FEM Analysis has been implemented employing ANSYS Workbench™; the achieved results as shown in Fig. 5b validate previous choice. Maximum contact pressure values are comparable with the analytical theory in Fig. 5a.

With higher loads the strain effects on the components increase and this causes a physical reduction of the gap h_1; for a certain (critical) load value, such gap would be reduced to zero, with the consequent unlocking of the cylinders, and (unwanted) torque transmission. The components where straining would generate such effects are: the ball bearings, cam shaft, cylinders, and secondarily, the fixed ring. Tolerances of the ball bearings, resulting in displacing the cam shaft, should also be considered. In order to calculate an optimal value for h_1, a FEM analysis simulating the critical load has been performed (see below Fig. 11b in the Results section). In this, the strain effects of the cam shaft, cylinders, and fixed ring have been considered. The effects of the ball bearings (due to both tolerances and stiffness) have been taken into account by considering a load value 1.5 the critical load permitted.

2.3 Dynamic Analysis

The theoretical torque dissipation has been calculated by means of a dynamic analysis of the mechanism supposing the worst case, i.e. the kinematic load is calculated according to static analysis but with dynamic load. Using the ball bearing theory [5] the torque dissipation caused by the rolling cylinders in dynamic condition M_m is:

$$M_m \approx 1.22 P_0^k \frac{\varsigma}{r_s}(r_c + r_s) \tag{9}$$

Where ζ represents the rolling friction factor [5]. An efficiency index, EI, has been approximated by the following relation:

$$EI = \frac{M - M_m}{M} \tag{10}$$

M is the input torque during the closure of the finger. By plotting EI, as shown in Fig. 5c, one can see that it is more sensitive to cylinder radius than to different material couplings and willing to use brass cylinders, high efficiency is achieved with radius larger than 1 mm (according to the results achieved by the static analysis).

External dimensions of the device are imposed by the requirement to fit all the actuation units in the size of a human hand. Once the static and dynamic analysis have been carried out, the diameter of the cylinders has been finally chosen: 3 mm; the kinematics analysis shows (cf. Fig. 4) that such value establishes a backlash lower than 6 degrees (not representing a significant problem for controllability): the value is comparable to standard backlash in commercial miniaturized actuators [22]. Returning to the static analysis, 1.5 mm radius ensures a critical load of about 150 N (cf. below Fig. 11b), which is found to be a suitable value for the proposed application, and a significant result considering the level of miniaturization. Moreover contact pressures (cf. Fig. 5) and the shear stress beneath the surfaces are lower than the yielding stress of the materials. The choice is also consistent with the dynamic analysis since a high theoretical efficiency is ensured.

2.4 Development and performance evaluation

CAD (ProEng™) tools have been used to design the mechanism, in order to minimize size and weight of the components. Based on previously mentioned analysis critical components such as motor shaft (2), cam (6) and fixed ring (1) have been machined using stainless steel (AISI 316 series) in order to ensure good resistance to stress, superficial and corrosive (due to lubricant) resistance. Cylinders have been machined in frictionless alloy (brass), in order to ensure low friction, suitable mechanical resistance, superficial hardness, resistance to corrosion and thermal stability of their properties. Less critical components have been machined in ERGAL aluminium (7075 series) alloy combining resistance and lightness. The clutching mechanism employs two compression springs (MeterSprings, model: D10210), while shafts are supported by two pairs (in Fig. 2) of miniaturized ball bearings (RMB, model: UL508X). Pictures of the developed mechanism are presented in Figs. 6a-b. The volume is about 5900 mm^3 (32 mm long, shafts included, 22 mm diameter, similar to a plastic bottle cap) and weighs 35 g.

Figure 6

The NBDM has been integrated in the SmartHand transradial prosthesis prototype [17] (see Fig. 7a), in a complete actuation mechanism (Fig. 6c) composed from the input to the output of:

1. a brushed DC motor [22], model 1319 012SR with integrated planetary gear head (491:1);

2. a spur gear couple;
3. **the NBDM developed**;
4. a 6.5 mm radius capstan, which is finally connected to a long rotational life resistive potentiometer Vishay Spectrol, model 157) able to measure the released tendon length;
5. 2 Hall effect proximity sensors (Allegro MicroSystems Inc., model A3213) acting as limit switches, that together with a magnet fixed on one spur gear limit the tendon release.

A stainless steel micro-cable tendon (Carl Stahl GmbH, 0.61 mm diameter, max tendon tension 152 N) is wound around the capstan, and runs into round wire spirals (Inner diameter 0.8 mm, outer diameter 1.6 mm, Tsukasa Machinery engineering Ltd, Japan) from the actuator output to the finger metacarpus (as in [7]). This design is completed by a round PCB on the top of the potentiometer, containing an active, 2nd order, low pass (bandwidth 150Hz), Sallen-Key filter circuit, to remove the noise from the position signal. Two identical actuation systems like the one described are housed in the palm of the SmartHand and employed to independently actuate the thumb and index fingers. For a detailed description of the hand refer to [17].

Figure 7

Tests have been carried out in order to evaluate the performances of the developed NBDM, on its own, integrated within the actuation unit, and finally in the hand. In particular the following issues have been investigated: (i) the efficiency of the NBDM, (ii) its critical load, (iii) the maximum tendon tension achievable, (iv) the efficacy of the non-back-drivability of the NBDM-finger system, and the consequent maximum grasp strength of the artificial hand.

2.4.1 Efficiency of the NBDM

The efficiency of the mechanism has been measured with the NBDM connected to the motor and the other actuation unit parts using the following set-up. The electrical wires of the brushed DC motor were directly connected to a voltage adjustable power supplier (Agilent, model: E3646A) also able to measure current absorption (1 mA resolution). One of the proximity sensors together with a magnet mounted on the output shaft was used to measure the output rotation period, by means of a digital oscilloscope (Tektronix: TDS 2024B) probe directly connected to the proximity sensor output. Input current absorption and speed of the NBDM output shaft have been therefore measured varying the supply voltage (1V steps), in two operational conditions: (i) no load and (ii) nominal load. The latter is intended as the mean load value required to close the artificial finger (i.e. 50 Nmm). Same measurements have been carried out without the NBDM, in order to compare results and therefore derive its efficiency.

Input current absorption and speed of the NBDM output shaft has been also measured varying the load (200 g steps) at maximum supply voltage. As well as being important for the calculation of the efficiency, this experiment has been useful for measuring the maximum achievable tendon tension by the actuation unit in the hand. The efficiency may be calculated considering the scheme in Fig. 8, where the energy balance is calculated as follows.

$$\eta = \frac{L_{out}}{L_{in}} = \frac{P_{out}}{P_{in}} \tag{11}$$

$$\mathrm{VI}\eta_e\eta_r\eta_{sg}\eta_{nbm} = C_r\omega \tag{12}$$

In this model the efficiency of the spur gear coupling is considered constant with load according to [20]. It is also assumed that η_e and η_r are constant with load and equal to the values provided in the manufacturer's data-sheet [22].

Figure 8

2.4.2 Critical load of the NBDM

The critical load has been measured as follows: the NBDM was assembled with the capstan, on which a steel cable was wound. The cable was connected to a 20 Kg (full scale) mono-axial load cell (Tedea Huntleigh, model: 1040), that has been used to force (by pulling the cable) the NBDM both in the clockwise and anticlockwise rotation direction, while its output was being acquired (1 KHz sampling) by an analogue acquisition PC board (National Instrument, model: PCI 6071E). This measurement has been repeated several times.

2.4.3 Efficacy of the system

With this term we refer to the capability of the developed NBMD of being non-back-drivable. In other words, its capacity to maintain the tendon tension once the power supply is switched off. This feature turns out to be very important while the mechanism is used for a prosthesis. Once the artificial hand had been assembled, i.e. with two NBDMs properly connected to the thumb and index fingers, a 41 mm diameter, 12 cm long, plastic (delrin) cylinder (225 g), has been grasped at maximum strength (bringing the motor in stall situation) by one of these fingers (i.e. the thumb). The motor supply has been switched-off afterward; meanwhile the tendon tension was continuously being measured (sampling frequency of 35Hz) by a micro-fabricated tendon tension sensor, based on strain gauges, housed in the fingertip, in series with the mechanical stop of the tendon (refer to [23] for details).

The capacity of maintaining the grip, when looking at the whole robotic hand, is important when considering its grasping capabilities when switched off (also considering safety features). To give an example we report the maximum load that the hand can grasp in such situation, measured using the following set-up. The cylinder connected by means of

a steel cable to the load cell previously mentioned, was grasped at maximum grip strength. The hand was then switched-off (simulating a real life situation) and the cylinder was pulled out along its axis direction (cf. arrow in Fig. 12b) at a relatively high speed (about 130 mm/s), with the carbon fibre palm facing upwards, while the load cell signal was acquired by the an analogue acquisition PC board. For this measurement fingers were covered with silicone tubes acting as a cosmetic covering and improving friction between fingers and the cylinder.

3. RESULTS

3.1 Efficiency of the NBDM

Graphs in Fig. 9a and Fig. 9b respectively show the input current absorption and speed of the output shaft varying the driving voltage (X axes), with no load (grey curves) and with nominal load (black curves), employing (solid curves) or not (dashed curves) the NBDM. As expected current absorption is higher and speed is lower when the NBDM is employed, than when it is not used; this in both no load and nominal load conditions.

Figure 9

Figure 10

Fig. 10a shows derived efficiency curves of the NBDM, function of the motor driving voltage, with no load (grey curve) and nominal load (black curve); the latter is compared with the theoretical curve (dashed curve). The points of the curves have been calculated starting from the previous measurements (Fig. 9a) and using Eq. (12).
Fig. 10b shows the supply current (solid black) and speed (solid grey) of the NBDM output shaft varying the load (resistant torque) at maximum supply voltage. The efficiency curve is therefore calculated using Eq. (12) and plotted (dashed line); this result is according to previous measurements in Fig.10a. The maximum efficiency value for the NBDM is about 0.95 in the load range 50 Nmm - 150 Nmm.

3.2 Critical load of the NBDM

The graph in Fig. 11a shows the typical curve obtained by forcing the output capstan as described in the methods section. The measured load at which the NBDM unlocks is about 150 N, i.e. about 1 Nm (both clockwise and anticlockwise directions). This value is according to a FEM analysis (Fig. 11b) performed in the same range of torque values, showing that the motor shaft teeth come in contact with a pair of cylinders, unlocking the brake.

Figure 11

3.3 Efficacy of the system

In Fig. 12a the tendon tension while the thumb is grasping at full strength a 41 mm diameter cylinder is plotted; the beginning of closure and the switch-off events are indicated. The capacity of maintaining the tendon tension is evident; no significant changes in the tendon tension value (due to backlash or elastic phenomenon) are found once the power is turned off. The measured maximum tendon tension is about 45 N. In Fig. 11b the tangential force required to extract the cylinder from the hand during power grasp as described in the methods section is shown. In the example slippage starts with 36 N of pulling force.

Figure 12

4. DISCUSSION

The proposed NBDM mechanism is aimed to being employed in all those robotic applications where it is fundamental to have a safe, miniaturized, low-cost, and high efficiency actuation unit, such as in artificial hand prostheses, humanoid robot hands, and generally in grippers. In particular it has been recently integrated into a transradial prosthetic hand, already in use for research in human-machine control interfaces. The field of application could be extended to industrial or non-clean environments, as the core of the mechanism is protected (unlike simple screw/lead screw couplings); this avoids infiltrations of dust and extraneous particles in general. In addition, by employing common flanged ball bearings, more protection could be achieved. Experiments have been carried out in order to evaluate the mechanical performances of the system, and results are here discussed.

With reference to the efficiency evaluation (cf. Section 2.4.1), it must be noted that with very low motor driving voltage values (1÷2 V), the theoretical and derived efficiency curves (in Fig. 10a) are significantly different. This is caused by unavoidable second order effects such as micro-machining drill imperfections, and eccentricities (causing irregular operation while running), that have affected the current and speed measurements (cf. Fig. 9). In the first two plotted points the measured values refer to mean values. Beyond the second point, secondary effects become insignificant and the NDBM shows a very high efficiency according to the theoretical value analytically calculated.

Current absorption and speed curves (cf. Fig. 9) employing or not employing the NBDM present similar trends. This implies that the efficiency is constant in the observed power supply range.

The maximum tendon tension achievable by the DC motor used is around 45N, whereas passively the NDBM could permit to correctly lift a 10 kg suitcase. The measured critical load of 150N is considered indeed, to be suitable for the

present application. To increase such value, e.g. for higher torque applications, the mechanism should be redesigned, by increasing the number of rolling elements in order to reduce the inner loads.

The capacity of being non-back-drivable (here defined efficiency) is evident by looking at Fig. 12a. It should be noted although, that such a feature is well demonstrated in the present system due to a correct combination of the stiffness of the transmission elements (finger, tendon, bowden cable, NBDM), where the NBDM is the stiffer element of the chain.

5. CONCLUSION

The authors have presented an innovative non-back-drivable mechanism based on wedge phenomena to be employed in all those robotic applications where it is fundamental to have a safe, miniaturized, low-cost, easy to assemble, and high efficiency actuation unit, such as in artificial hand prostheses, humanoid robot hands, and generally in grippers. In particular the system has been developed and fitted in the SmartHand transradial prosthesis, where the autonomy of the entire system, the available grasping force, the weight and size, to a large extent depend on the performances of the actuator unit.

After detailed kinematics, static and dynamic analyses, the proposed system has been developed and evaluated in terms of efficiency, critical load, maximum tendon tension achievable with the finger, and efficacy of the non-back-drivability. The backlash is about 6 degrees. The measured maximum efficiency is about 0.95 in the load range 50 Nmm - 150 Nmm; the load at which the NBDM unlocks is about 150N, i.e. about 1Nm. The capacity of maintaining the tendon tension has been experimentally evidenced and the measured maximum tendon tension of the actuation unit is about 45 N. Such performances are suitable for the challenging, miniaturized and low-power application but could be further improved in order to employ the component in other fields of robotics.

AKNOWLEDGMENTS

Authors would like to thank L. Bassi Luciani and S.P. Murdoch for their precious work. This work was supported by the SMARTHAND project (NMP4-CT#2006-33423).

REFERENCES

[1] J.L. Pons, E. Rocon, R. Ceres, D. Reynaerts, B. Saro, S. Levin, W. Van Moorleghem, The MANUS-HAND Dextrous Robotics Upper Limb Prosthesis: Mechanical and Manipulation Aspects, Autonomous Robots **16** (2004) 143-163.

[2] H. Kawasaki, T. Komatsu, K. Uchiyama, T. Kurimoto, Dexterous anthropomorphic robot hand with distributed tactile sensor: Gifu hand II, IEEE International Conference on Systems, Man, and Cybernetics SMC (1999) 2782-787.

[3] Y. Matsuoka, The Mechanisms in a Humanoid Robot Hand, Autonomous Robots **4** (2) (1997) 199-209.

[4] V. Bégoc, C. Durand, S. Krut, E. Dombre, F. Pierrot, On the Form-Closure Capability of Robotic Underactuated Hands, 9th International Conference on Control, Automation, Robotics and Vision ICARCV (2006) 2011-2018.

[5] E. Funaioli, A. Maggiore, U. Meneghetti, Lezioni di Meccanica Applicata alle Macchine, vol. I, Patron Editore, Bologna, (1987).

[6] C. M. Light, P. H. Chappell, Development of a lightweight and adaptable multiple-axis hand prosthesis, Medical Engineering & Physics **22** (2000) 679-684.

[7] M.C. Carrozza, G. Cappiello, S. Micera, B.B. Edin, L. Beccai, C. Cipriani, Design of a cybernetic hand for perception and action, Biological Cybernetics **95** (6) (2006) 629-644.

[8] B. Massa, S. Roccella, M. C. Carrozza, P. Dario, Design and development of an underactuated prosthetic hand, IEEE International Conference on Robotics and Automation ICRA (2002).

[9] N. Dechev, W.L. Cleghorn, S. Naumann, Multiple Finger, Passive Adaptive Grasp Prosthetic Hand, Journal of Mechanism and Machine Theory **36** (10) (2001) 1157-1173.

[10] <http://www.touchbionics.com>, (accessed August 2009)

[11] P. J. Kyberd, M. Evans, S. te Winkel, An Intelligent Anthropomorphic Hand, with Automatic Grasp, Robotica **16** (1998) 531-536.

[12] P. Kyberd, O. Holland, P. Chappell, S. Smith, R. Tregidgo, P. Bagwell, M. Snaith, MARCUS: A Two Degree of Freedom Hand Prosthesis with hierarchical grip control, IEEE Trans on Rehabilitation Engineering **3** (1) (1995) 70-76.

[13] I. I. Artobolevesky, Mechanism in Modern Engineering Design, vol. II –Lever Mechanism–, MIR Publishers, Moscow (1976).

[14] J. Chu, D. Jung, Y. Lee, Design and control of a multifunction myoelectric hand with new adaptive grasping and self-locking mechanisms, IEEE International Conference on Robotics and Automation ICRA (2008) 743 -748.

[15] <http://www.ottobockus.com>, (accessed August 2009)

[16] Otto Bock Healthcare IP GMBH & Co, International Patent PTC,WO 2007/076795 A1 Clutch Module for prostheses (2007).

[17] C. Cipriani, M. Controzzi, M. C. Carrozza, Objectives, Criteria and Methods for the Design of the SmartHand Transradial Prosthesis, Robotica, First View, Issue (2009) 1-9 DOI 10.1017/S0263574709990750

[18] W. Beitz, K.-H. Kuttner, Dubbel - Manuale di Ingegneria Meccanica, Springer (1984).

[19] M. T. Mason, J. K. Salisbury Jr., Robot hands and the mechanics of manipulation, MIT Press Cambridge MA USA (1985).

[20] R. Juvinall, K. Marshek, Fundamentals of Machine Component Design, third ed., John Wiley & Sons. Inc. (1991).

[21] K. L. Johnson, Contact Mechanics, Cambridge University Press (1985).

[22] Faulhaber Group Catalogue (2008).

[23] C. Cipriani, F. Zaccone, G. Stellin, L. Beccai, G. Cappiello, M.C. Carrozza, P. Dario, Closed Loop Controller for a Bio-inspired Multi-fingered Underactuated Prosthesis, IEEE International Conference on Robotics and Automation ICRA (2006) 2111-2116.

List of captions:

Fig. 1 a) Lead screw pair. b) Worm gear. c) Conventional free wheel.

Fig. 2 a) Non-back-drivable mechanism exploded view. b) Parametric scheme and core section.

Fig. 3 a) Zero position. b-c) Two steps of backlash in the direct motion of the mechanism; springs are not presented.

Fig. 4 Influences of the cylinder radius on the backlash of the mechanism graphs. Arrows show the procedure in order to find the backlash in the direct motion (from the motor shaft to the output). The input parameter is the diameter of the cylinder in the left graph; this gives the value for gap h_1. Then, as explained in the text, gap h_2 can be chosen, and must be larger than h_1. Once chosen h_2, this is used as the input of the right graph, functional for determining the total backlash of the device g_2.

Fig. 5 a) Analytical static analysis based on Hertz theory. Influence of cylinder radius and material type on contact pressures. Figures show that the optimal radius is about 1.5 mm. b) FEA investigation on the contact pressures; results are according to analytical ones. c) Theoretical efficiency index EI as function of cylinder radius and material couplings.

Fig. 6 NBDM developed prototype. A) Internal view. B) Comparison with one Eurocent. C) Integration within the actuation unit.

Fig. 7 The SmartHand prototype integrating two non-back-drivable mechanisms. A) Dorsum view of the hand with the NBDMs highlighted. B) SmartHand during clinical evaluation with an amputee. This picture shows the comparison between the natural hand and the artificial one in which two NBDMs have been integrated.

Fig. 8 Actuation unit efficiency transmission scheme.

Fig. 9 a) No load and nominal load (50 Nmm) measured current consumption employing or not the NBDM in the transmission chain. b) No load and nominal load (50 Nmm) speed measured employing or not the NBDM in the transmission chain.

Fig. 10 a) Derived no load and nominal load (50 Nmm) efficiency of the NBDM and theoretical nominal load efficiency. b) Measured speed, current consumption and derived efficiency, depending on load.

Fig. 11 Critical load. a) Load cell forcing the mechanism: the arrow indicates the tendon force at which the NBDM unlocks becoming back-drivable. b) FEM analysis in the range of load.

Fig. 12 a) Typical tendon tension of the thumb while grasping a 41mm diameter cylinder. b) Typical load force versus time when a grasped cylinder (as shown in the small picture) is pulled out at constant speed.

Figures:

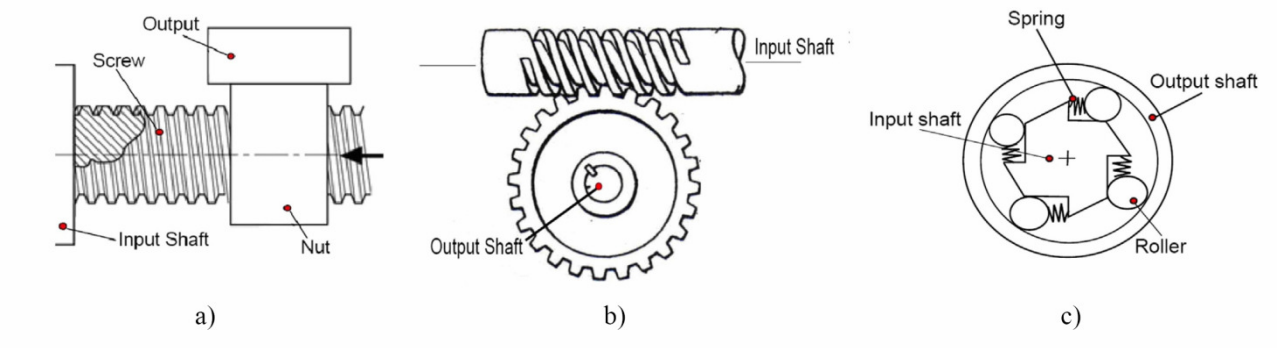
Output
Screw
Input Shaft
Nut
Input Shaft
Output Shaft
Spring
Output shaft
Input shaft
Roller
a)
b)
c)

Fig. 1

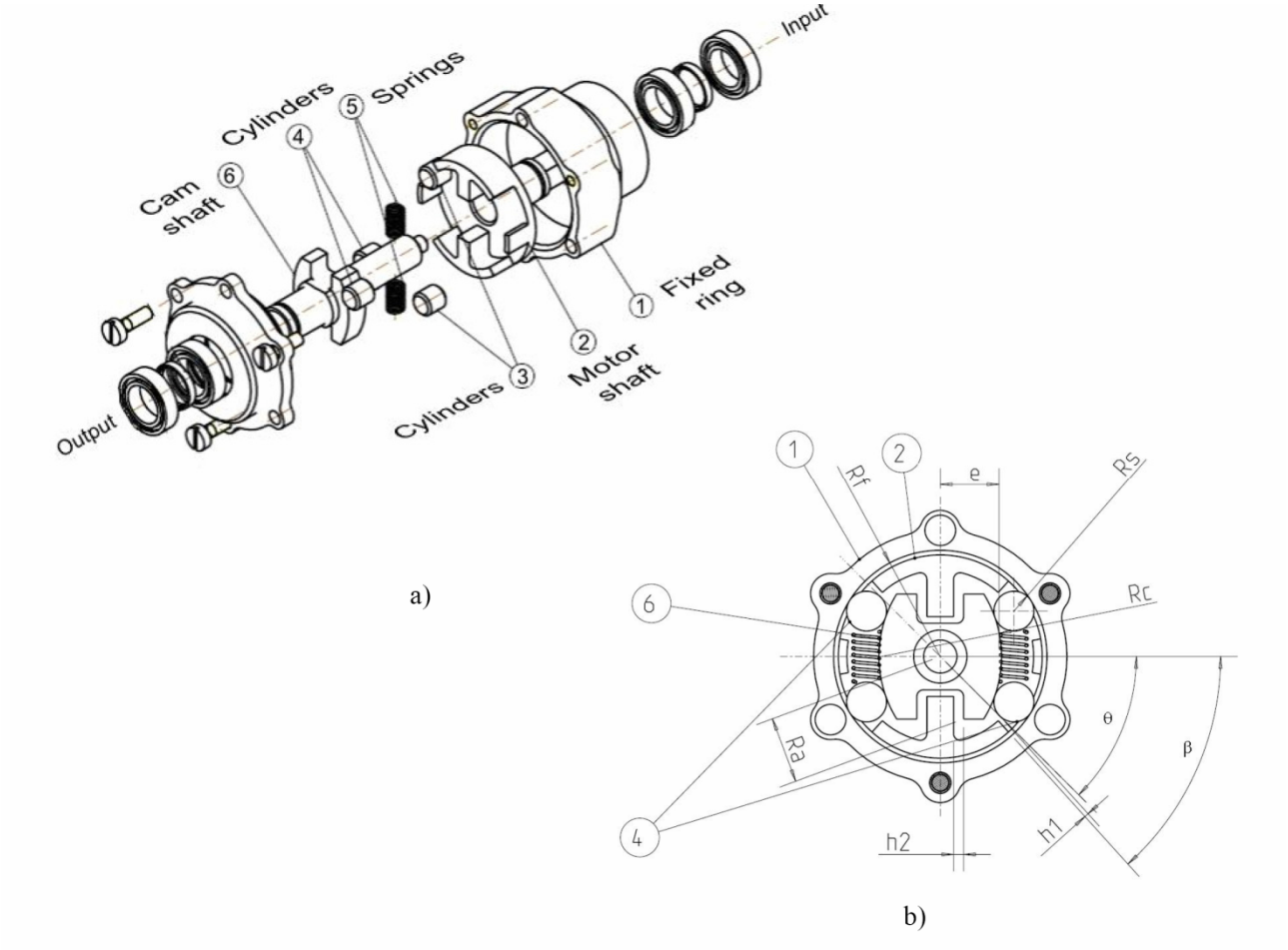
Input
Cylinders
Springs
Cam shaft
Fixed ring
Motor shaft
Cylinders
Output
a)
Rf
Rs
e
Rc
Ra
θ
β
h2
h1
b)

Fig. 2

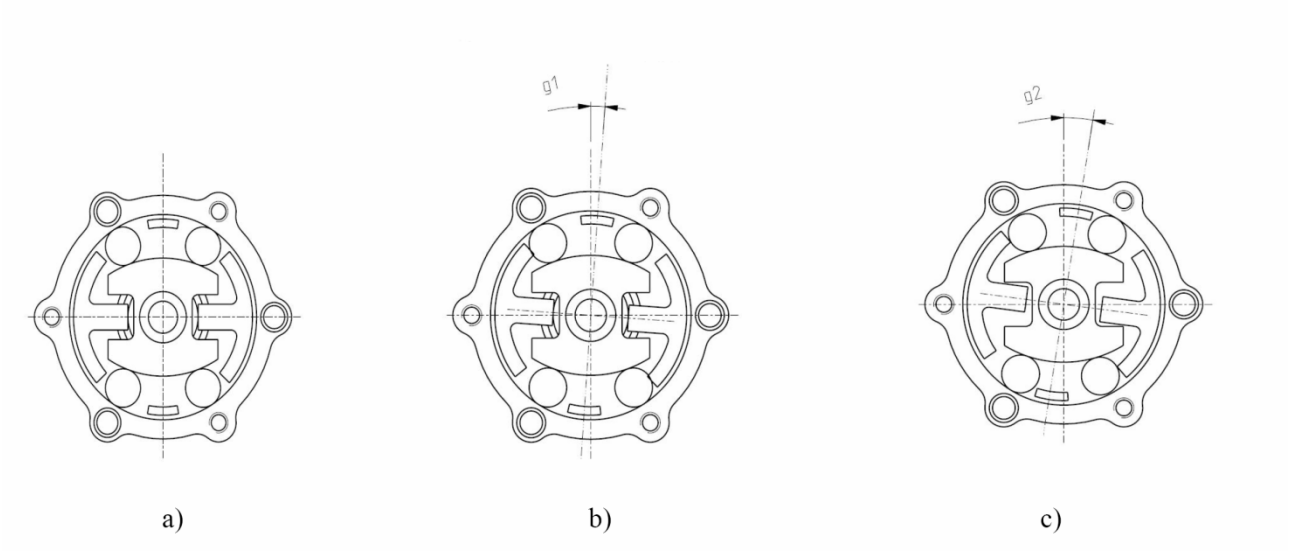
g1
g2
a)
b)
c)

Fig. 3

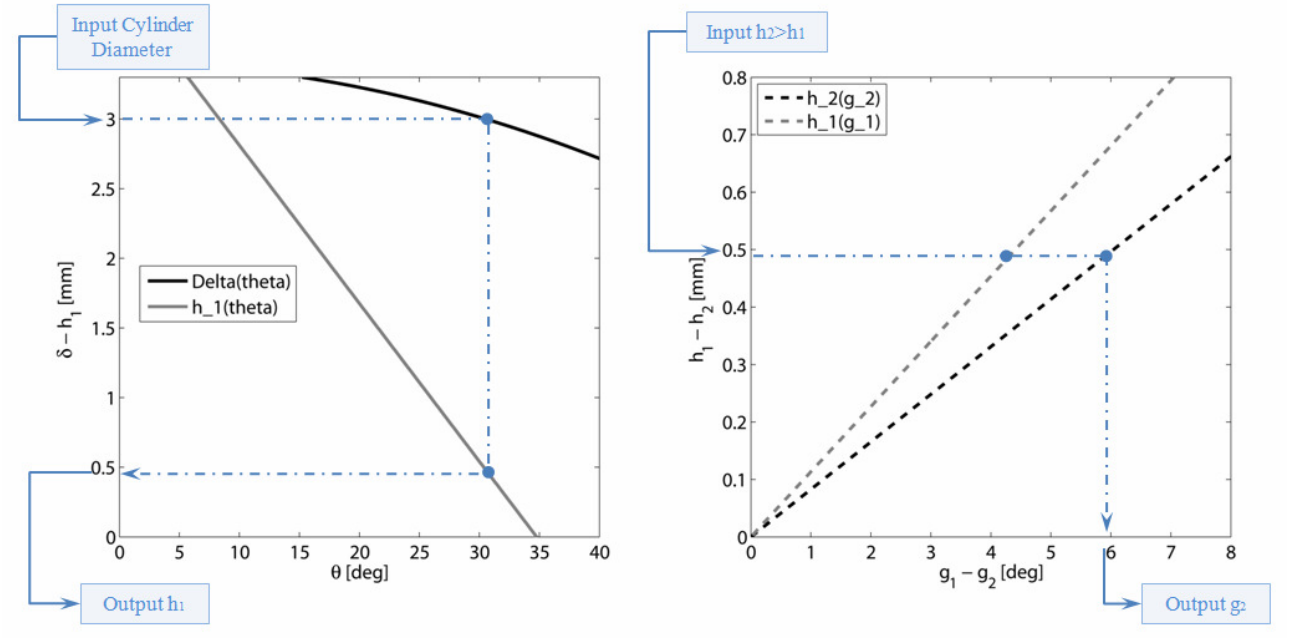
Input Cylinder Diameter
Delta(theta)
h_1(theta)
δ – h1 [mm]
θ [deg]
Output h1
Input h2>h1
h_2(g_2)
h_1(g_1)
h1 – h2 [mm]
g1 – g2 [deg]
Output g2

Fig. 4

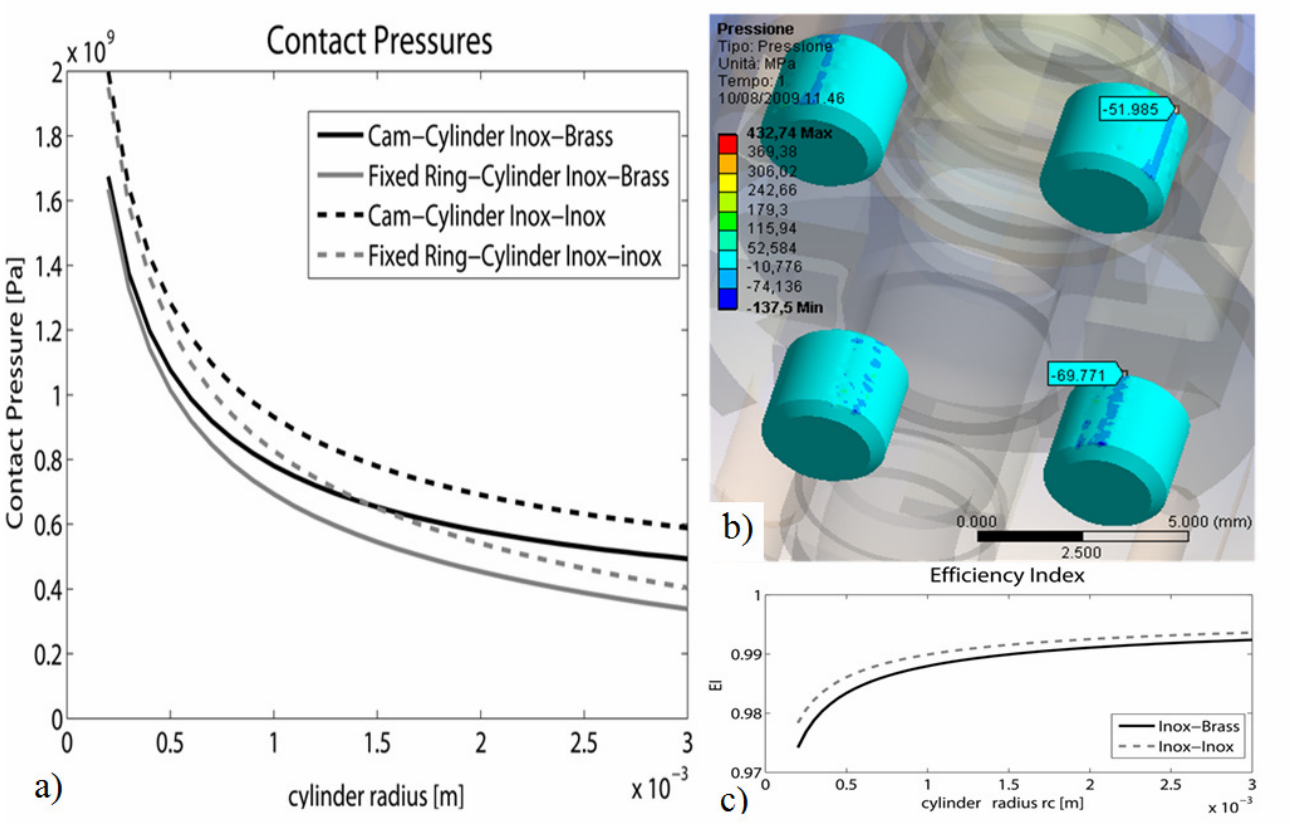
Contact Pressures
x 10^9
Contact Pressure [Pa]
cylinder radius [m]
x 10^-3
Cam–Cylinder Inox–Brass
Fixed Ring–Cylinder Inox–Brass
Cam–Cylinder Inox–Inox
Fixed Ring–Cylinder Inox–inox
a)
Pressione
Tipo: Pressione
Unità: MPa
Tempo: 1
10/08/2009 11.46
432,74 Max
369,38
306,02
242,66
179,3
115,94
52,584
-10,776
-74,136
-137,5 Min
-51.985
-69.771
0.000
5.000 (mm)
2.500
b)
Efficiency Index
EI
cylinder radius rc [m]
x 10^-3
Inox–Brass
Inox–Inox
c)

Fig. 5

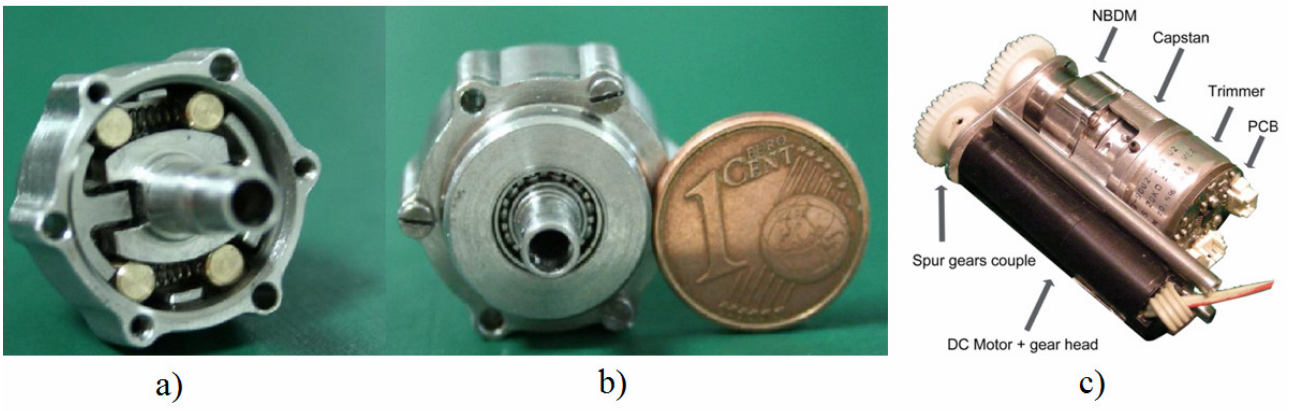
NBDM
Capstan
Trimmer
PCB
Spur gears couple
DC Motor + gear head
a)
b)
c)

Fig. 6

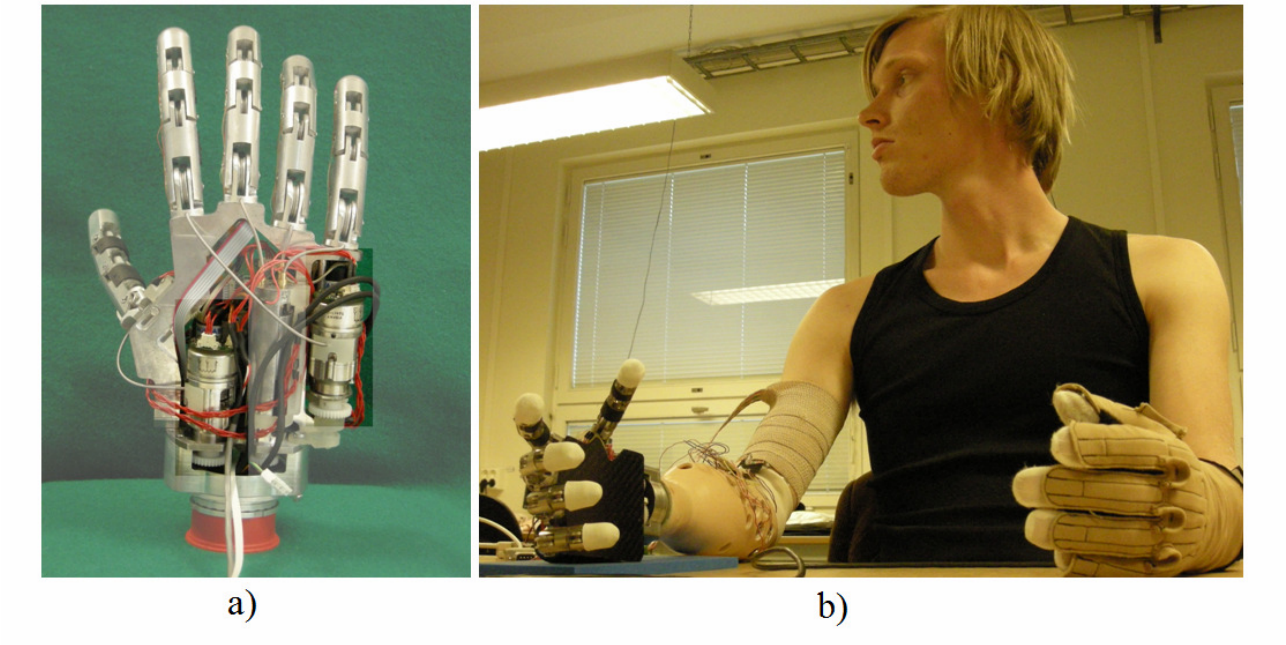
a)
b)

Fig. 7

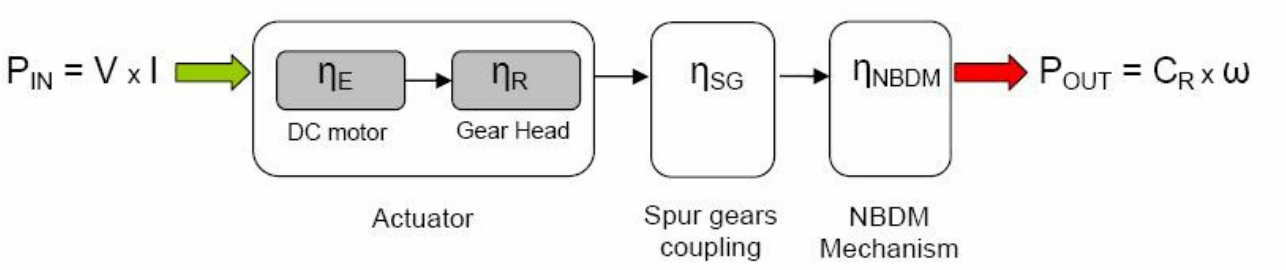
$P_{IN} = V \times I$
η_E
DC motor
η_R
Gear Head
Actuator
η_{SG}
Spur gears coupling
η_{NBDM}
NBDM Mechanism
$P_{OUT} = C_R \times \omega$

Fig. 8

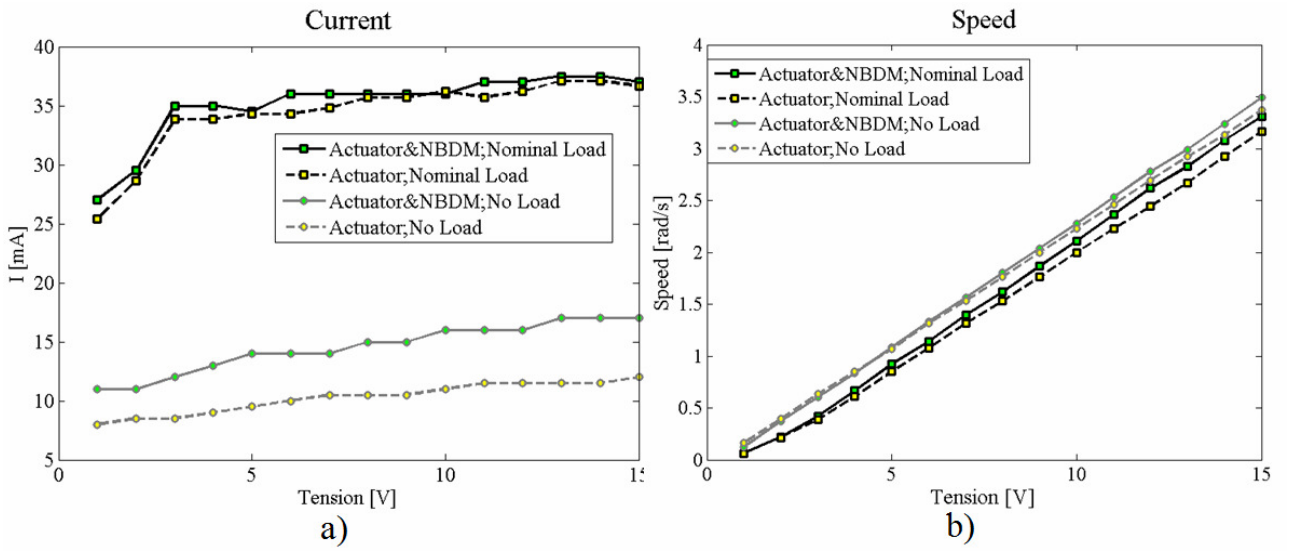
Current
I [mA]
Tension [V]
Actuator&NBDM;Nominal Load
Actuator;Nominal Load
Actuator&NBDM;No Load
Actuator;No Load
a)
Speed
Speed [rad/s]
Tension [V]
Actuator&NBDM;Nominal Load
Actuator;Nominal Load
Actuator&NBDM;No Load
Actuator;No Load
b)

Fig. 9

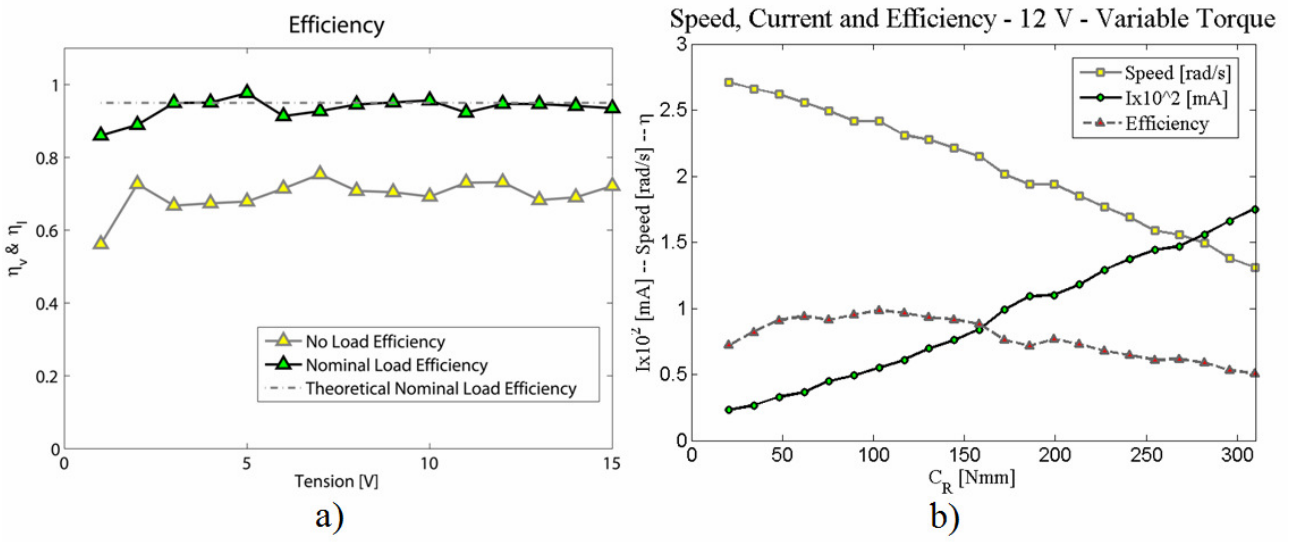
Efficiency
η_v & η_I
Tension [V]
No Load Efficiency
Nominal Load Efficiency
Theoretical Nominal Load Efficiency
a)
Speed, Current and Efficiency - 12 V - Variable Torque
$Ix10^2$ [mA] -- Speed [rad/s] -- η
C_R [Nmm]
Speed [rad/s]
Ix10^2 [mA]
Efficiency
b)

Fig. 10

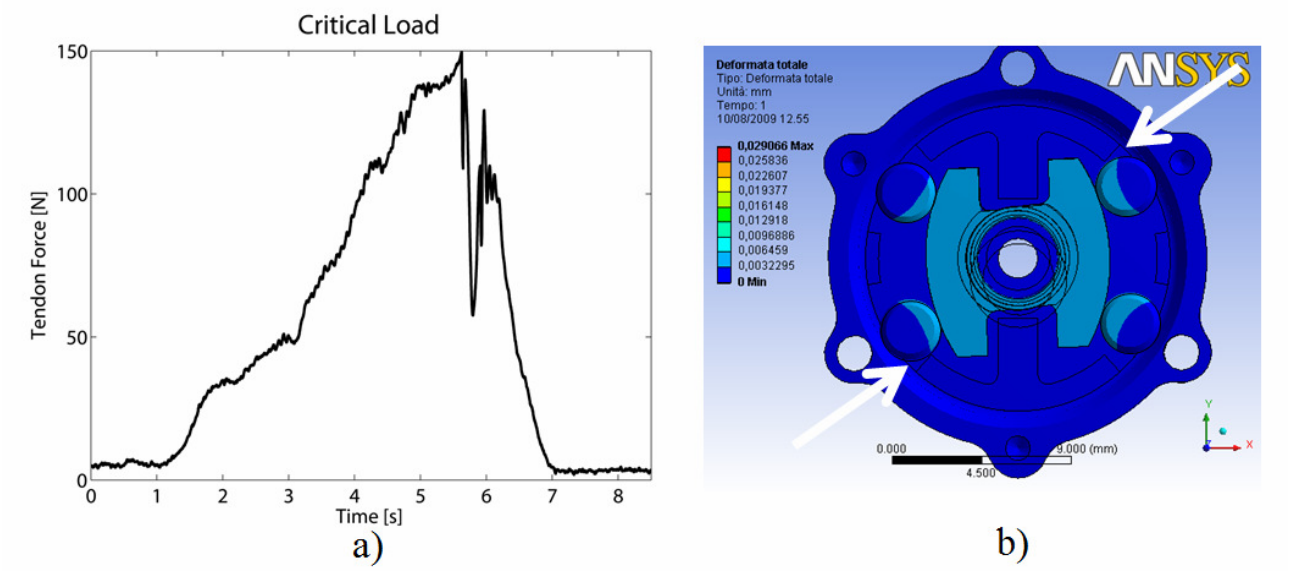
Critical Load
Tendon Force [N]
Time [s]
a)
Deformata totale
Tipo: Deformata totale
Unità: mm
Tempo: 1
10/08/2009 12.55
0,029066 Max
0,025836
0,022607
0,019377
0,016148
0,012918
0,0096886
0,006459
0,0032295
0 Min
ANSYS
0.000
4.500
9.000 (mm)
b)

Fig. 11

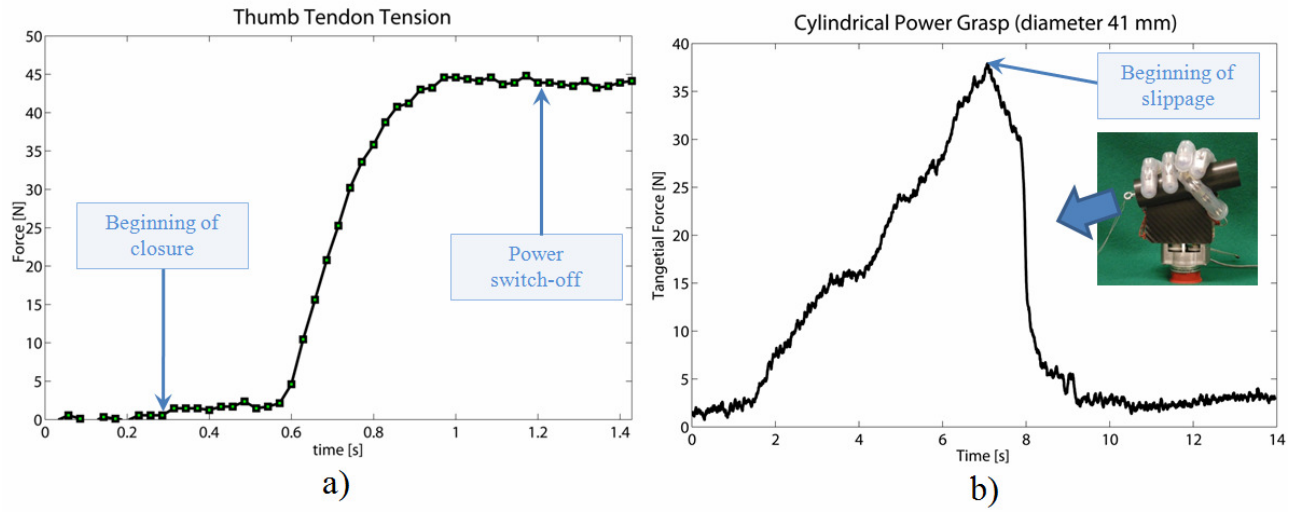
Thumb Tendon Tension
Force [N]
time [s]
Beginning of closure
Power switch-off
a)
Cylindrical Power Grasp (diameter 41 mm)
Tangetial Force [N]
Time [s]
Beginning of slippage
b)

Fig. 12